Solid-State Emission and Aggregate Emission of Aroyl-S,N-Ketene Acetals Are Controlled and Tuned by Their Substitution Pattern

Lukas Biesen,[a] Dennis Woschko,[b] Christoph Janiak,[b] and Thomas J. J. Müller*[a]

Abstract: Aroyl-S,N-ketene acetals are a novel highly diverse class of aggregation-induced emission fluorogens (AIEgens) with a plethora of interesting properties. An expanded compound library of more than 110 dyes set the stage for the first qualitative control and tuneability of all aspects of their photophysical properties. The interplay of substituents not only allows tuning and prediction of the emission color, but also of the intensity, and quantum yields both in solids and in the aggregated state; these can be rationalized by scrutinizing intermolecular interactions in the crystalline solid state.

Introduction

Functional fluorescent dyes are immensely relevant in numerous fields of high-tech application[1] such as sensors and fluorescence probes,[2] medicinal imaging and therapy,[3] or OLEDs.[4] As acknowledged by IUPAC in 2019 upon declaring it as one of the "top ten emerging technologies in chemistry",[5] aggregation-induced emission (AIE)[6] or aggregation-induced enhanced emission (AIEE)[7] has quickly become a highly versatile enabling tool in all these areas. Both aspects exploit the suppression of nonradiative excited-state decay by restricting intramolecular motions (RIM)[8] or by restricted access to conical intersections (RACI) upon dye aggregated.[9] From an applicational perspective, solid-state emission is the most common form of dye usage.[10] As the demands for novel chromophore systems grow more and more specific, these dyes have to be tailor-made. On the Mount Olympus of functional dyes are therefore systems whose properties can be decidedly fine-tuned by shape and form.[11] Especially the control of solid-state emission[12] or AIE behavior[13] plays a crucial role as they mostly define their applicational potential. The field of AIE-active dyes is largely dominated by tetraphenylethene derivatives[14] but in the last few years, novel polar heterocyclic systems such as indolone merocyanines,[15] quinoxalines,[16] isoquinolines[17] or aroyl-S,N-ketene acetals[18] have been disclosed, which also show solid-state emission control on a small scale with respect of the solid-state emission color.

After recently introducing aroyl-S,N-ketene acetals as a novel class of AIEgens,[18] we predominantly expanded the diversity-oriented synthesis by concatenating Suzuki cross-coupling to generate novel bi-[19] or multichromphores[20] for studying communication pathways between chromophores and for enabling energy transfer processes. Yet, in constituting the chromophores aroyl-S,N-ketene acetals per se revealed a pattern and correlations of the photophysical properties we now set out to nail down. As proven and emphasized previously, the occurrence of AIE is strongly contingent on the N-benzyl substitution.[18] Herein, we report the expansion of the aroyl-S,N-ketene acetal library together with in-depth analysis of the photophysical properties that allows to understand and control solid-state and aggregation-induced emission through the substitution pattern.
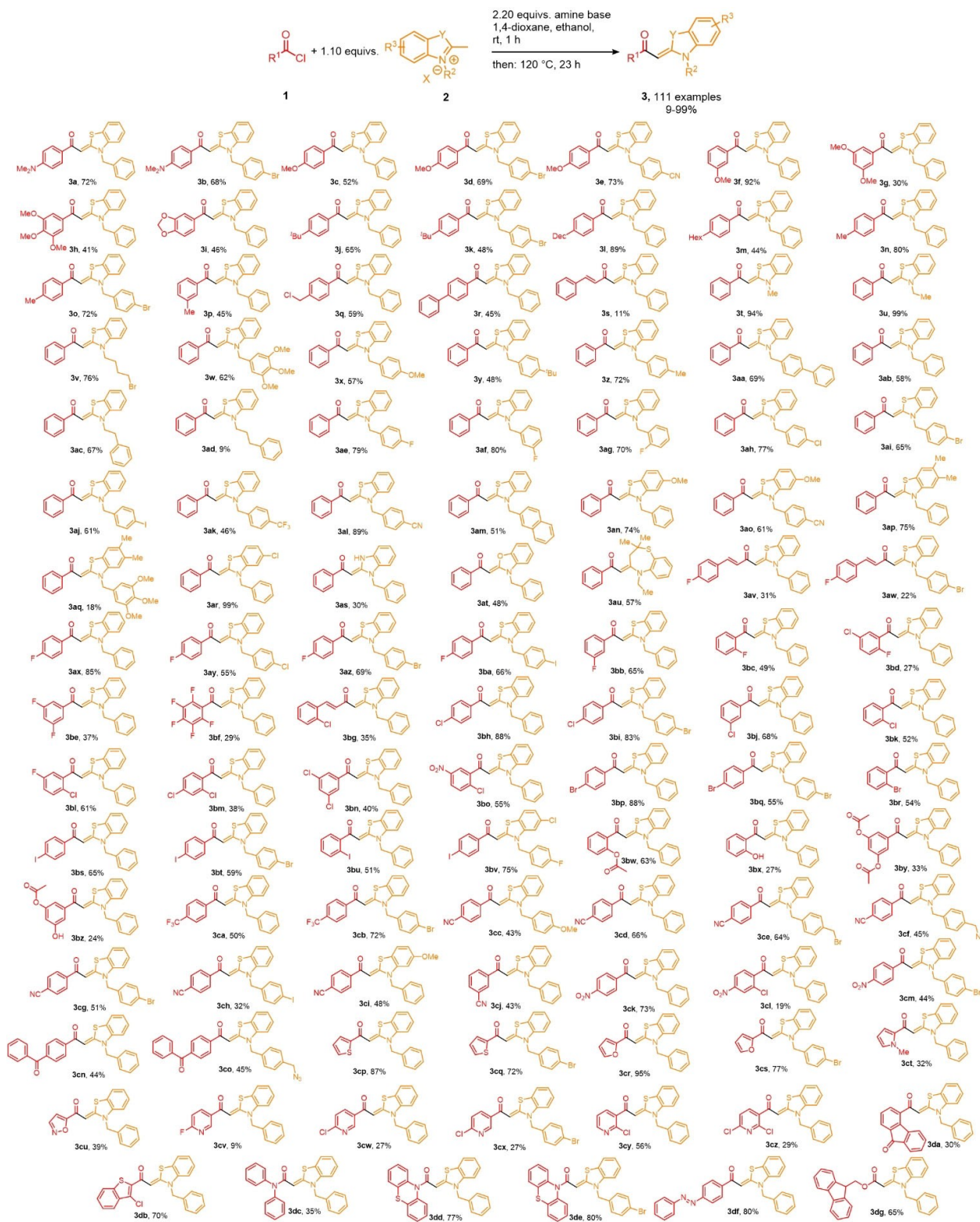
Results and Discussion

Synthesis

As a primary synthetic tool, the already well-established[18] straightforward condensation by amine base mediated addition-elimination of acid chlorides **1** and benzothiazolium salts **2** in 1,4-dioxane and ethanol provides 111 compounds in poor to excellent yields (Scheme 1). With exception of **3a** and **3b**, where diisopropylethylamine was employed in pure 1,4-dioxane, triethylamine was used as a base. Furthermore, for the chloromethyl substituted compound **3q**, ethanol must be omitted as co-solvent. It was possible to implement any kind of substituents either electron-donating and electron-withdrawing substituents in the ortho, meta, and para positions of both benzyl and aroyl moiety, also bearing multiple substituents is possible as well as various heterocycles. Substituents can also be placed at the benzothiazole core so that almost no synthetic

[a] L. Biesen, Prof. Dr. T. J. J. Müller
Institut für Organische Chemie und Makromolekulare Chemie
Heinrich-Heine-Universität Düsseldorf
Universitätsstraße 1, 40225 Düsseldorf (Germany)
E-mail: ThomasJJ.Mueller@hhu.de

[b] D. Woschko, Prof. Dr. C. Janiak
Institut für Anorganische Chemie und Strukturchemie
Heinrich-Heine-Universität Düsseldorf
Universitätsstraße 1, 40225 Düsseldorf (Germany)
E-mail: Janiak@uni-duesseldorf.de

Supporting information for this article is available on the WWW under https://doi.org/10.1002/chem.202202579

Chem. Eur. J. **2022**, 28, e202202579 (1 of 12)

© 2022 The Authors. Chemistry - A European Journal published by Wiley-VCH GmbH

Chemistry–A European Journal

Research Article
doi.org/10.1002/chem.202202579

Chemistry Europe
European Chemical
Societies Publishing

Scheme 1. Synthesis of aroyl-*S,N*-ketene acetals **3**. All reactions were performed on a 1.0 mmol scale: **1** (1.0 mmol), **2** (1.1 mmol), and amine base (2.2 mmol) in 1,4-dioxanes/ethanol (5:2, 7.0 mL) were stirred at room temperature for 1 h, then at 120°C for 23 h. Yields given are after purification by flash chromatography on silica gel. For examples **3a** and **3b**, diisopropylethylamine instead of triethylamine was used as amine base and 1,4-dioxane was used as sole solvent, which also applied for **3q**).

Chemistry–A European Journal

Research Article
doi.org/10.1002/chem.202202579

Chemistry Europe
European Chemical
Societies Publishing

limitations for preparing aroyl-*S,N*-ketene acetals can be found and three points of diversity are readily feasible. Only *N-tert*-butyl and *N*-phenyl aroyl-*S,N*-ketene acetals could not be realized (for details, see Section 3.2 in the Supporting Information).

Absorption and fluorescence in ethanol

Most of the investigated aroyl-*S,N*-ketene acetals have lowest energy absorption maxima in a narrow range from 375 to 420 nm. Typically, aroyl-*S,N*-ketene acetals do not fluoresce in solution, however there are some exceptions to this rule. Most prominently, dimethylamino-substituted compounds **3a** and **3b** show significant luminescence with quantum yield $\Phi_f =$ 0.20. Furthermore, halochromism can be observed with a pronounced bathochromic shift both in absorption and emission spectra, thus, revealing a pK_a value of 5.79 and reversible protonation characteristics (Figures S110–S112 in the Supporting Information). Generally speaking, aroyl-*S,N*-ketene acetals with electron-donating substituents or enhanced electron density on the aroyl moiety, such as dyes **3a**, **3b**, or **3r**, luminesce in solution. Additionally, if the benzyl moiety represents a secondary chromophore, as in case for *N*-trimethoxy benzyl (**3w**), *N*-methyl biphenyl (**3aa**), or *N*-methyl naphthyl derivatives(**3am**), a weak blue luminescence can be observed.

Rainbow tuning of solid-state emission

The enormous expansion of the aroyl-*S,N*-ketene acetal library naturally offers the possibility to further expand the rainbow tuning of solid-state emission color by varying the substituents

at aroyl moiety (Figure 1). Starting from deep blue for the *o*-bromo substituted derivative **3br** ($\lambda_{em} = 446$ nm) reaching over to green (**3ba**, $\lambda_{em} = 522$ nm), yellow (**3ay**, $\lambda_{em} = 563$ nm) and orange (**3cd**, $\lambda_{em} = 593$ nm) to red for the *p*-nitro substituted derivative **3ck** ($\lambda_{em} = 646$ nm). It is even possible to push solid-state emission ever further into the NIR region by 2-chloro-4-nitro substitution (**3cl**, $\lambda_{em} = 731$ nm). Consequently, any color needed for any application can be achieved by carefully choosing the correct arrangement of substituents.

Controlling solid-state and aggregation-induced emission

Comparing the ortho*,* meta*, and* para *positions of the aroyl moiety*

As previously shown for related aroyl-*S,N*-ketene acetal AIEgens, ethanol/water mixtures turned out to be better suited for assessing the AIE properties in comparison to aqueous mixtures of other organic solvents, such as THF, acetonitrile, acetone.[18–20] Commencing with the aroyl moiety bearing substituent R^1, the influence on both solid-state emission and AIE behavior is tremendous as on the emission color. Methoxy and aliphatic groups on R^1 give rise to blue emission in the aggregated state ($\lambda_{em} = 470$–490 nm), halogenated derivatives luminesce blue-greenish ($\lambda_{em} = 500$ nm) as well as most of the heterocyclic moieties, like thienyl or furyl substituted aroyl-*S,N*-ketene acetals. However, placing two halides at the substituent R^1 causes a bathochromic shift of AIE emission to green as seen for the trifluoromethyl substituent ($\lambda_{em} = 520$–540 nm). Hydroxy or cyano substituents on R^1 further lead to a red shift thus resulting in a yellow emission color ($\lambda_{em} = 550$–560 nm). Using benzophenone as an R^1 substituent, as well as isoxazole,
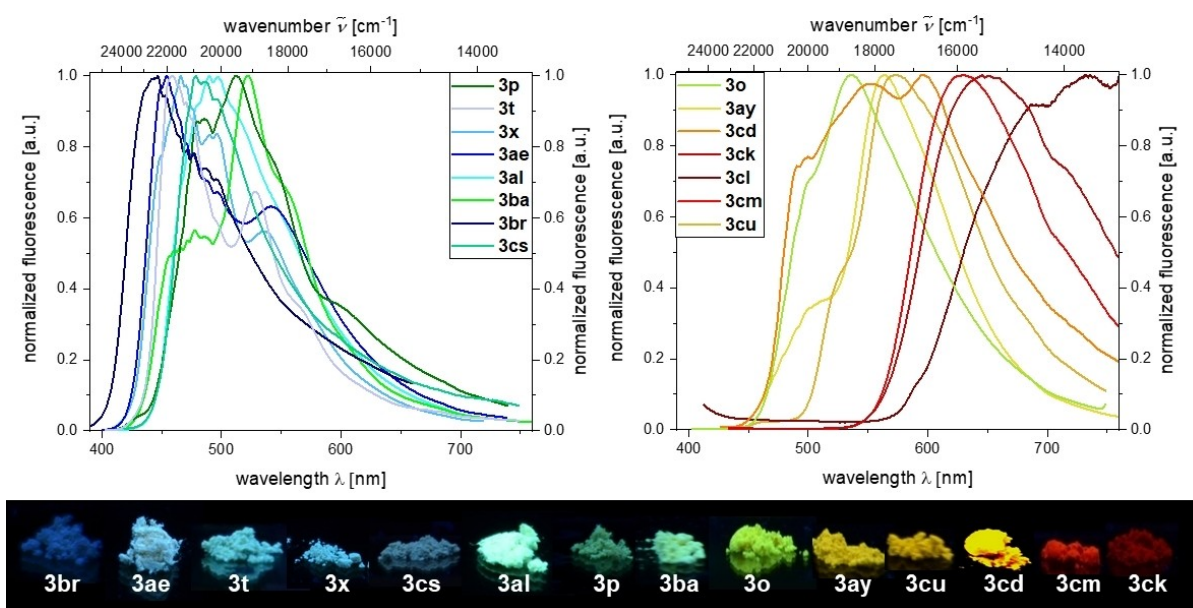

Figure 1. Top: Normalized solid-state emission spectra of selected aroyl-*S,N*-ketene acetals **3** ($\lambda_{ex} = \lambda_{abs,max}$ at $T = 298$ K); bottom: solid-state fluorescence colors of selected aroyl-*S,N*-ketene acetal derivatives **3** ($\lambda_{ex} = 365$ nm) revealing emission-color tuning by substitution pattern.

Chemistry–A European Journal

Research Article
doi.org/10.1002/chem.202202579

Chemistry Europe
European Chemical
Societies Publishing

provides emission of orange light in aggregated state (λ_{em} = 570–590 nm). Finally, the most pronounced redshift is observed for the fluorenone substituted dye (λ_{em} = 600 nm). However, for too strongly electron-withdrawing substituents, no AIE behavior can be found, as for nitro-substituted derivatives **3 ck**, **3 cl**, and **3 cm** (for AIE investigations of all compounds, see Chapter 6 of the Supporting Information).

The comparison of the *ortho*, *meta*, and *para* substitution discloses a distinct influence on the emission characteristics in the aggregates and the solid state. While *ortho* and *para* substitution affect luminescence color in a similar fashion, *ortho* substitution leads to a small hypsochromic shift in the solid-state emission color and simultaneously diminishes the solid-state quantum yield from 0.09 to 0.05. This may also be ascribed to a twisting of the aroyl moiety out of plane when bearing substituents at the *ortho* position as supported by DFT calculations[18] (e.g., Figure S69 or S72). For the AIE behavior, the same effect on quantum yields is observed, furthermore, the *ortho*-substituted derivative **3 bk** starts to aggregate at higher water fractions in comparison to *para*-substituted dye **3 bh**. Bringing *meta*-substituted derivative **3 bj** to the picture, an unexpected behavior becomes apparent.

While quantum yields in the solid-state are quite similar, the emission is significantly bathochromically shifted to greenish color (λ_{em} = 536 nm). The same can be observed for the AIE color, which is also shifted to longer wavelengths. Additionally, the quantum yield upon aggregation increases from 0.09 for *ortho* substitution to 0.13 for the *meta* isomer. These effects are confirmed by all investigated consanguineous lines of substituted chromophores, such as the three fluoro-substituted isomers **3 ax**, **bb** and **bc** or their analogues (Figure 2; for further examples, see, Chapter 6 in the Supporting Information).

AIE control through aliphatic chain length

Additionally, the starting point of aggregation can be controlled by varying the aliphatic chain length at the R^1 substituent (Figure 3).

While the *p*-tolyl derivative **3 n** starts to form aggregates at water fractions above 80%, the *p*-hexyl-substituted dye **3 m** already forms aggregates at water fractions of 70% and a decyl chain at *para* position of the aroyl moiety (**3 l**) leads to the formation of aggregates at water fractions of 60%. This early onset of aggregation at lower water fractions is in accordance with the increased hydrophobicity of longer aliphatic chains. Playing also into this part is the enhanced steric hindrance at dye approximation caused by the increased aliphatic chain

Figure 2. Top: Emission spectra of **3 bh**, **3 bj**, and **3 bk** in ethanol/water mixtures upon increasing water content (recorded at T = 298 K, c = 10^{-7} M, λ_{ex} = $\lambda_{abs,max}$). Second row: solid-state fluorescence colors of selected aroyl-*S,N*-ketene acetal derivatives **3 bh**, **3 bj** and **3 bk** (λ_{ex} = 365 nm). Bottom: Normalized solid-state emission spectra of selected aroyl-*S,N*-ketene acetals **3** (λ_{ex} = $\lambda_{abs,max}$ at T = 298 K).

Chemistry–A European Journal

Research Article
doi.org/10.1002/chem.202202579

Chemistry Europe
European Chemical
Societies Publishing

Figure 3. Emission spectra of **3n**, **3m**, and **3l** in ethanol/water mixtures of increasing water content (recorded at $T = 298$ K, $c = 10^{-7}$ M, $\lambda_{ex} = \lambda_{abs,max}$). Bottom: Visualization of **3n**, **3m**, and **3l** in ethanol/water mixtures with increasing water content ($\lambda_{ex} = 365$ nm).
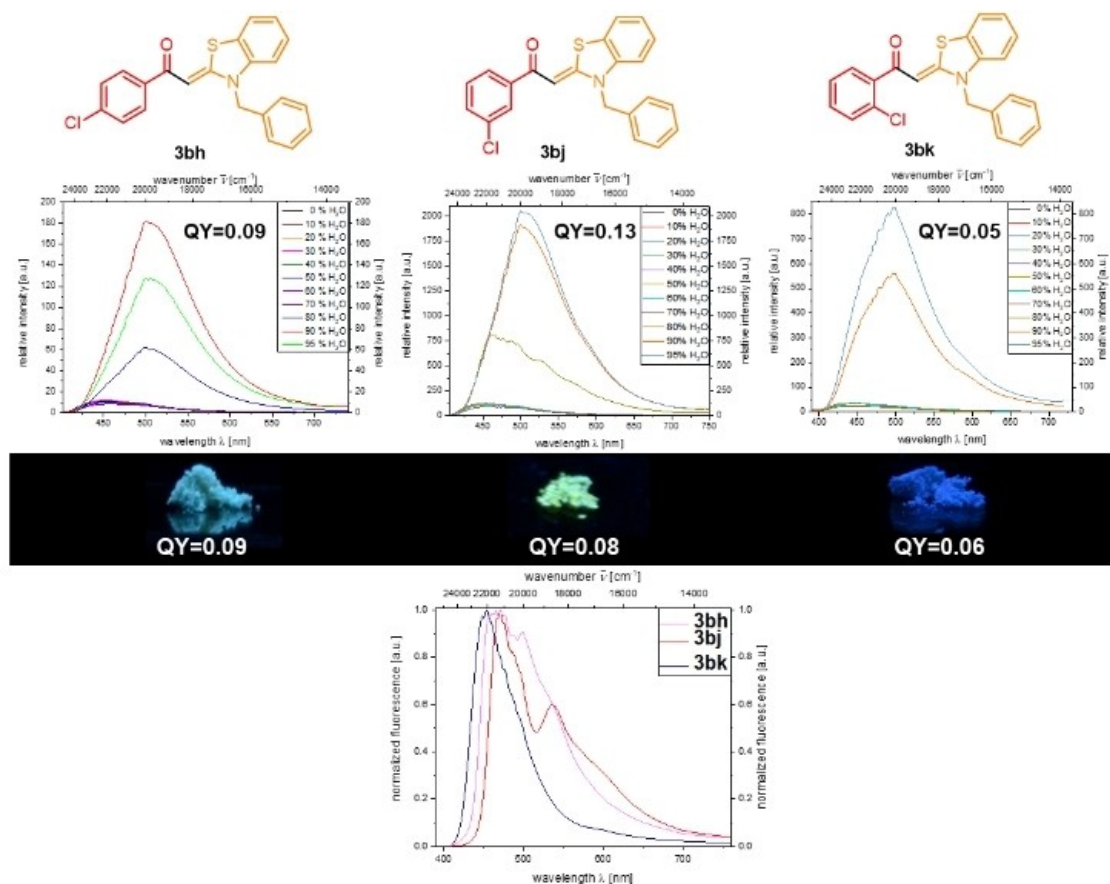

Figure 4. Top: Emission spectra of **3bd**, **3bl**, **3bm**, and **3bn** in ethanol/water mixtures upon increasing water content (recorded at $T = 298$ K, $c = 10^{-7}$ M, $\lambda_{ex} = \lambda_{abs,max}$). Second row: Visualization of **3bd**, **3bl**, **3bm**, and **3bn** in ethanol/water mixtures with increasing water content ($\lambda_{ex} = 365$ nm). Third row: solid-state fluorescence colors of **3bd**, **3bl**, **3bm**, and **3bn** ($\lambda_{ex} = 365$ nm). Bottom left: Normalized solid-state emission spectra ($\lambda_{ex} = \lambda_{abs,max}$ at $T = 298$ K); right: comparison of AIE emission intensities.

Chemistry–A European Journal

Research Article
doi.org/10.1002/chem.202202579

Chemistry
Europe
European Chemical
Societies Publishing

length, which consequently diminishes π-π-stacking and, thus, further elevating AIE effects. Introducing an aliphatic chain increases Φ_f from 0.06 (**3n**) to 0.14 (**3m**), further elongation of the aliphatic chain causes a gradual drop of the quantum yield to 0.09 (**3l**) probably due to a poorer solubility of the dyes in more polar solvent mixtures (Figure 3).

Influence of multiple substituents at aroyl moiety

When analyzing the influence of multiple substituents, the main influence can be relegated to the position of the substituents. Most dominant for photophysical properties of aroyl-*S,N*-ketene acetals is the *para* positioning of two or more substituents. *Para* substituents control emission properties both in the solid state and in the aggregated form regardless of other substituents. In the absence of *para*-substituents, the *ortho* position defines photophysical properties while the *meta* position only exerts a minor influence. This is unequivocally shown by comparing 2-chloro-4-nitro substituted derivative **3cl** and 2-chloro-5-nitro substituted derivative **3bo**. The *p*-nitro substitution causes a massively bathochromic shift of the solid-state emission up to 731 nm and, as typical for the solely nitro-substituted com-

pound, no AIE behavior could be observed. However, placing the nitro-substituent at the 5-position, the *o*-chloro substituent effects a far less bathochromic shift of the emission maximum for **3cl** ($\lambda_{em} = 622$ nm) and only a weak AIE behavior can be observed (Figure 4). Comparison of chloro-fluoro-substituted derivatives **3bd** and **3bl** further supports the postulates. The smaller fluorine substituent placed in *ortho* position, furnishes a significantly higher quantum yield both in aggregated form (0.10 vs. 0.04) and in the solid state (0.15 vs. 0.06). Furthermore, emission maxima are hypsochromically shifted by changing from 2-fluoro to 2-chloro substitution ($\lambda_{em} = 489$ vs. 455 nm). Upon aggregation the shift of the emission maximum reverts and causes a redshift for the 2-chloro substitution. The comparison of 2,4-chloro and 3,5-chloro substitution elegantly shows the dominance of *para* position as the 2,4-disubstituted compound behaves similarly as the 4-chloro-substituted derivative with respect to AIE behavior and solid-state emission properties. Only the quantum yield in the aggregated state is diminished and can be likely ascribed to an out of plane twist of the aroyl moiety caused to the 2-chloro substitution. For 3,5-dichloro substitution, a similar behavior as for the *m*-chloro derivative for both solid-state emission and AIE is seen as well as a bathochromic shift to green. However, the AIE quantum
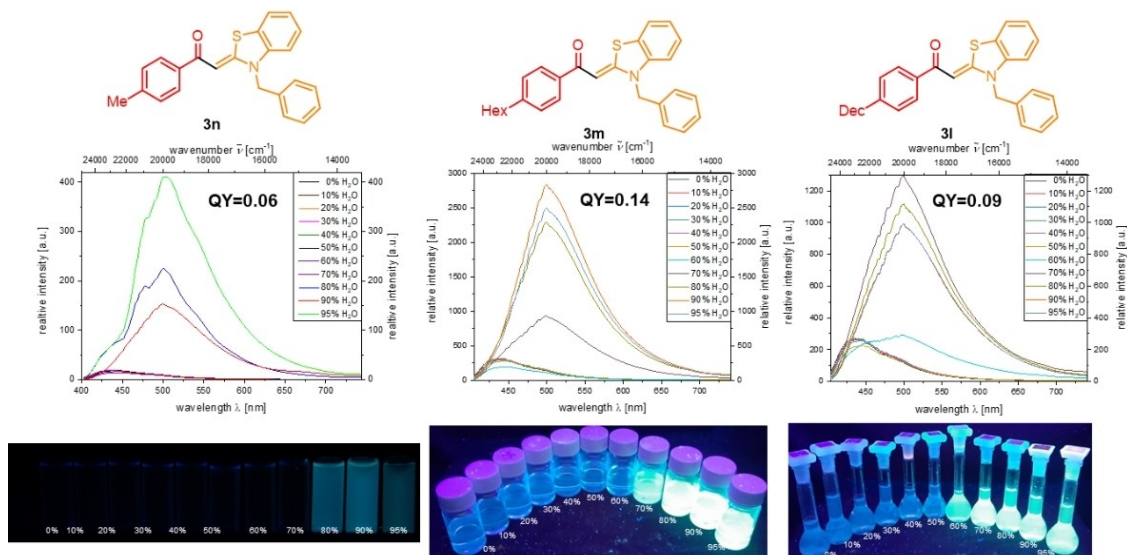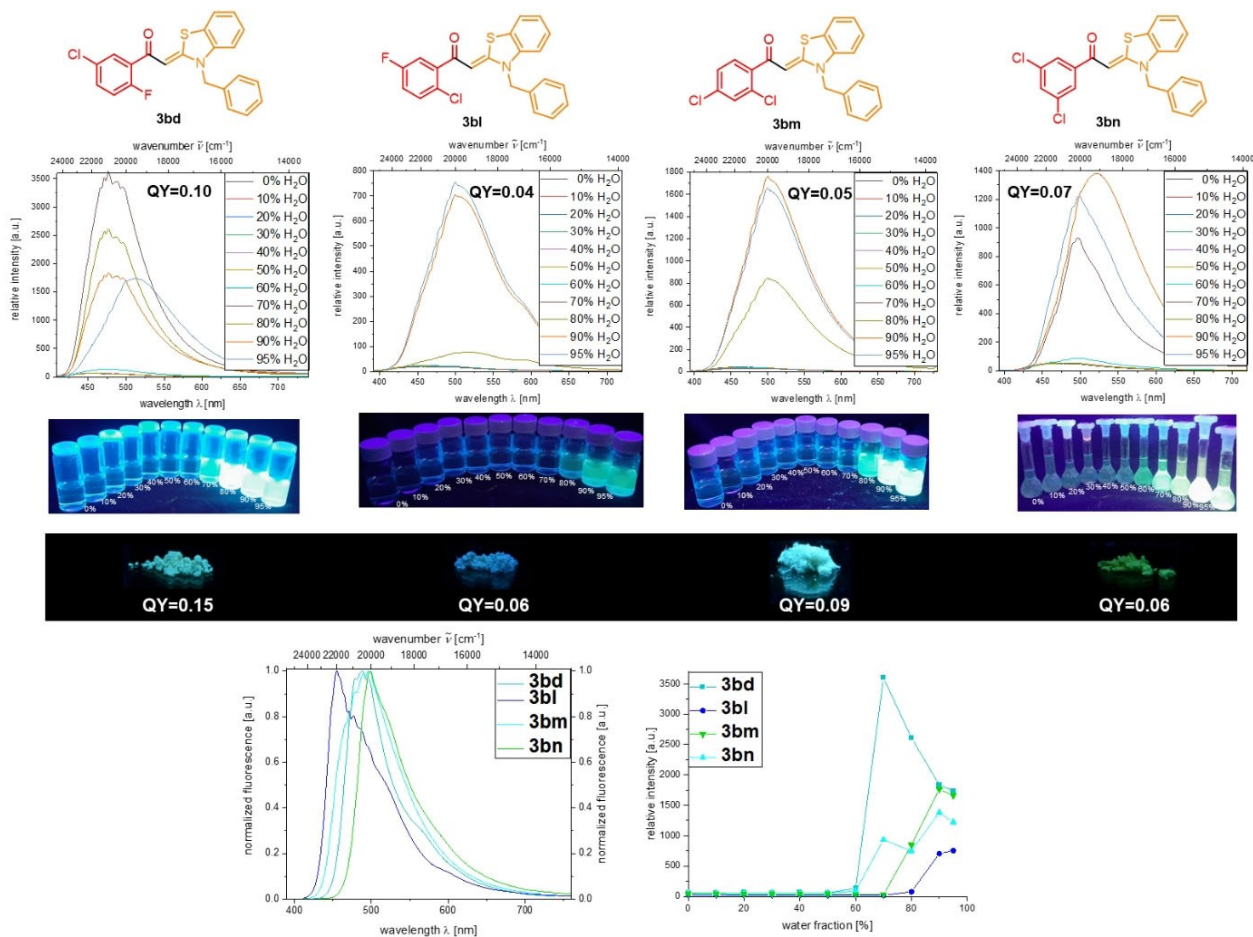

Figure 5. Top: Emission spectra of **3an**, **3ap**, **3ab**, and **3ar** in ethanol/water mixtures upon increasing water content (recorded at $T = 298$ K, $c = 10^{-7}$ M, $\lambda_{ex} = \lambda_{abs,max}$). Second row: Visualization of **3an**, **3ap**, **3ab**, and **3ar** in ethanol/water mixtures with increasing water content ($\lambda_{ex} = 365$ nm). Third row: solid-state fluorescence colors of **3an**, **3ap**, **3ab**, and **3ar** ($\lambda_{ex} = 365$ nm). Bottom left: Normalized solid-state emission spectra ($\lambda_{ex} = \lambda_{abs,max}$ at $T = 298$ K); right: comparison of AIE emission intensities.

Chemistry–A European Journal

Research Article
doi.org/10.1002/chem.202202579

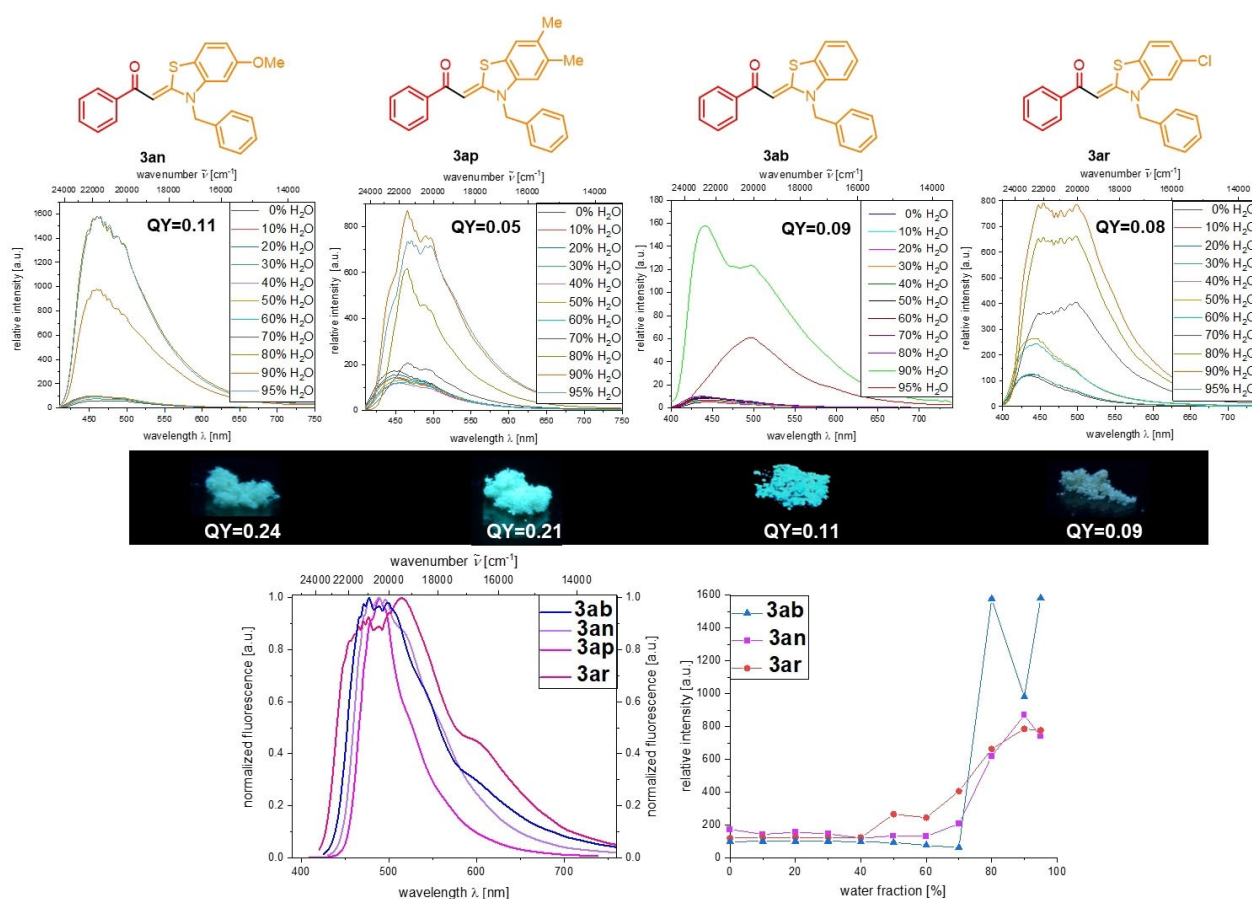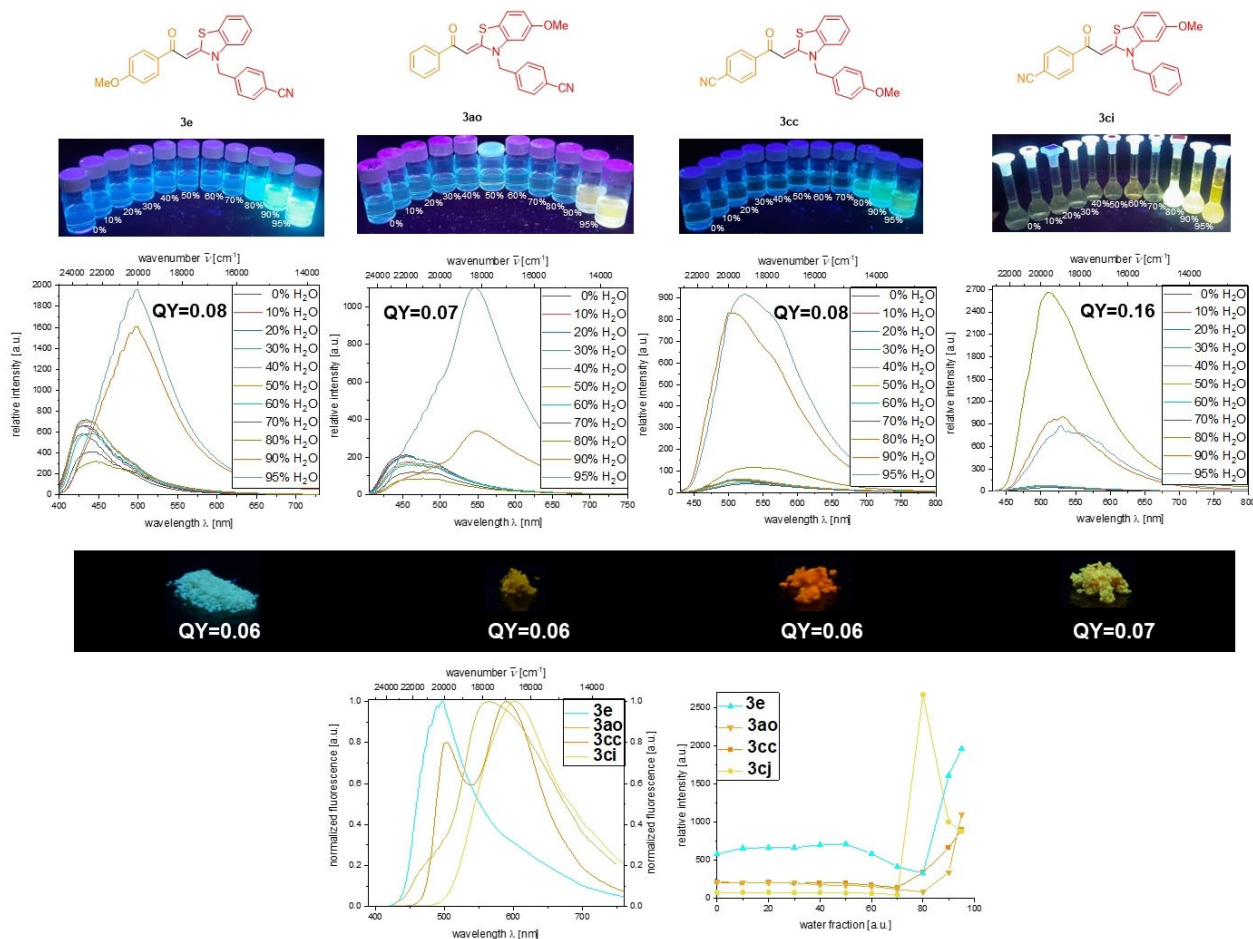Chemistry
Europe
European Chemical
Societies Publishing

Figure 6. Top: Emission spectra of **3e**, **3ao**, **3cc**, and **3ci** in ethanol/water mixtures upon increasing water content (recorded at $T = 298$ K, $c = 10^{-7}$ M, $\lambda_{ex} = \lambda_{abs,max}$). Second row: Visualization of **3e**, **3ao**, **3cc**, and **3ci** in ethanol/water mixtures with increasing water content ($\lambda_{ex} = 365$ nm). Third row: solid-state fluorescence colors of **3e**, **3ao**, **3cc**, and **3ci** ($\lambda_{ex} = 365$ nm). Bottom left: Normalized solid-state emission spectra ($\lambda_{ex} = \lambda_{abs,max}$ at $T = 298$ K); right: comparison of AIE emission intensities.

yield increases to 0.07 while solid-state quantum yields drop to 0.06 (Figure 4; for details, see Chapter 6 Supporting Information).

Influence of substituents at benzothiazole core

Variation of the substitution pattern R^3 on the benzothiazole moiety reveals a different kind of influence. While an effect on the emission color in the solid state or in the aggregates remains absent, only for the electron-withdrawing chloro substituent (**3ar**), a small bathochromic shift in the aggregate and in the solid state can be detected. Regarding the quantum yield upon aggregation, electron-withdrawing chloro substituents (**3ar**) cause a small decrease, whereas electron-donating substituents like methoxy substituents (**3an**) slightly increase Φ_f. In the case of two methyl groups at the benzothiazole core (**3ap**), Φ_f is attenuated as caused by the poor solubility of the dye. Most interestingly, for both, dimethyl substituted derivative **3ap** and chloro-substituted compound **3ar**, upon aggregation, a second maximum appears at higher wavelengths and addi-

tionally, prior the induction of aggregation the luminescence of both chromophores is more pronounced than for comparable aroyl-*S,N*-ketene acetals. The by far major influence of benzothiazole substitution is inevitably exerted on the solid-state emission quantum yield. For electron-withdrawing substituents (**3ar**), the quantum yield is slightly reduced to 0.09 in comparison to $\Phi_f = 0.11$ for the unsubstituted derivative **3ab**. For dimethyl-substituted derivative **3ap**, however, Φ_f is nearly doubled in the solid state ($\Phi_f = 0.21$) and for methoxy-substituted derivative **3an**, the quantum yield is even further increased to $\Phi_f = 0.24$ (Figure 5).

Circulating the substituents

Finally, all the previously discussed effects will be considered and combined and, therefore, a cyano and a methoxy substituent are placed at different substitution positions. Although all four aroyl-*S,N*-ketene acetals are regioisomers, the photophysical properties differ greatly. Regarding the solid-state emission properties, a methoxy substituent at the *para*

Chemistry–A European Journal

Research Article
doi.org/10.1002/chem.202202579

Chemistry Europe
European Chemical
Societies Publishing

position of R[1] leads to a blue emission in the solid state (**3e**, λ_{em} = 497 nm). In absence of substituents on aroyl moiety R[1] (**3ao**), the solid-state emission band is significantly bathochromically shifted resulting in a dark yellow emission, which is ascribed to a changed geometry due to the benzothiazole-benzyl substitution pattern. Placing a cyano substituent at the aroyl R[1] and a methoxy substituent at the benzyl group R[2], an orange solid-state emission (**3cc**, λ_{em} = 590 nm) is generated caused by the dominant influence of *p*-cyano-aroyl moiety. If the methoxy substituent changes position to the benzothiazole moiety R[3] (**3ci**), the emission is further bathochromically shifted to 602 nm. For the solid-state emission quantum yield, no significant differences are found due to leveling of the influence of the different substituents as on the one hand, cyano substituents on the aroyl moiety reduce quantum yields but on the other hand, the methoxy substituent at the benzothiazole increases quantum yield. Therefore, compared quantum yields in the same range are found (Figure 6).

The AIE behavior is also greatly influenced by altering the substituents' positions. Dye **3e** shows quite a similar behavior compared to the solely methoxy substituted derivative **3c** with blue emission upon aggregation at water fractions above 80% with Φ_f = 0.08 and, therefore, quite identical to Φ_f of **3c**. If both substituents simply switch positions, Φ_f does not change at all and again, aggregation starts at water fractions above 80%, which is typical for aroyl-*S,N*-ketene acetals with substituents at the aroyl and benzyl moiety if the hydrophobic behavior is not affected. Compared to the solely cyano substituted derivative **3cd**, the AIE bands are significantly hypsochromically shifted due to the methoxy-benzyl substituent consequently leading to a green AIE color. In the case of aroyl-*S,N*-ketene acetal **3ao**, the emission is drastically shifted

bathochromically upon aggregation, from initially λ_{em} = 450–550 nm after aggregation and simultaneously, the aggregation commences only at higher water fractions, again typical for a benzothiazole-benzyl substitution pattern. The leveling of both substituents, the quantum yield ranges again in the same magnitude as discussed before. Aroyl-*S,N*-ketene acetal **3ci** starts to aggregate at a water fraction of 80% as well, revealing a yellow AIE color at λ_{em} = 550 nm caused by the p-cyano substituent at the aroyl moiety. But the interplay of substituents of **3ci**, especially the influence of the methoxy substituent at the benzothiazole core leads to a significant increase of Φ_f upon aggregation to 0.16 (Figure 6). All those exemplary postulates are further confirmed by the photophysical data of the 111 derivatives encompassing the aroyl-*S,N*-ketene acetal library (see Chapters 5 and 6 in the Supporting Information). Yet, we did not observe a significant influence of the substitution pattern on the fluorescence lifetime τ. Therefore, this aspect was not considered further.[18]

Crystal structures

Fortunately, single crystals of selected aroyl-*S,N*-ketene acetals were obtained and structural characteristics in the solid state could be studied (Figure 7). While the aroyl and benzothiazole moiety arrange coplanarily, the benzyl group is oriented out of plane. Only for the chloro-substituted derivative **3ar**, the phenyl ring of the aroyl moiety is slightly twisted out of planarity. Standard *N*-benzyl aroyl-*S,N*-ketene acetals crystallize in the monoclinic space group $P2_1/n$. In the case of an *N*-methyl substitution, the orthorhombic space group *Pbca* is found and in the case of benzothiazepine derivative **3au** a tetragonal space group I_4 can be determined (Figure 7).
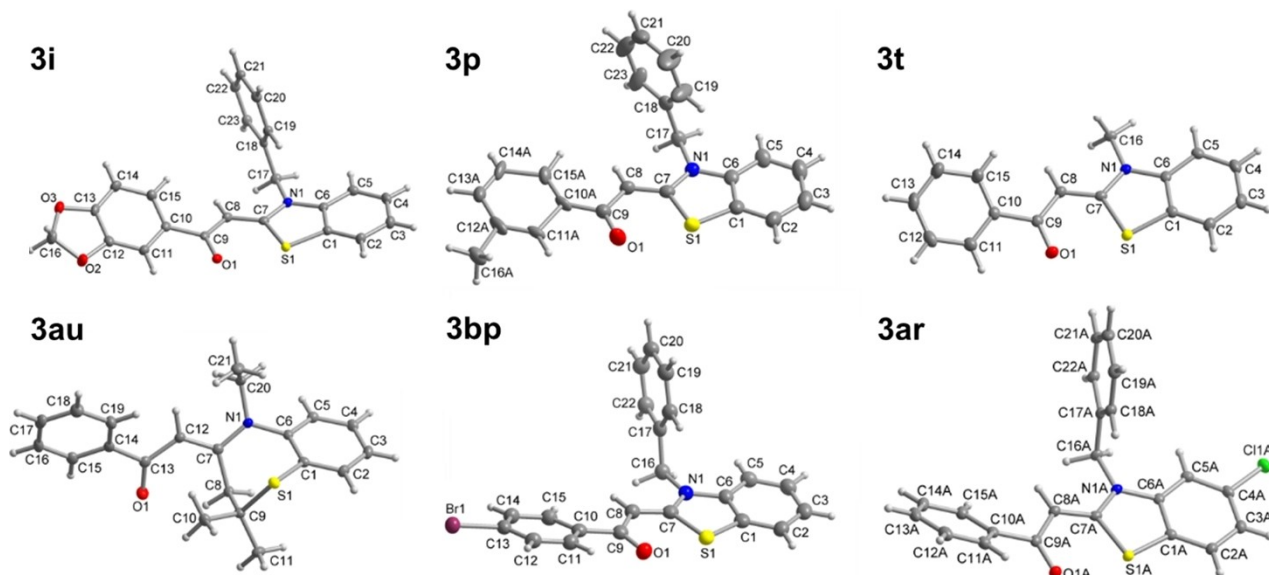
Figure 7. Molecular structures of selected aroyl-*S,N*-ketene acetals in the crystal (50% thermal ellipsoids). For the structures of **3j**, **3y**, **3cp** and **3cq**, see Figure 9, below. Enlarged drawings with atom numbering, presentation and discussion of the supramolecular packing can be found in Chapter 7 of the Supporting Information. Deposition Numbers 2190350, 2190351, 2190352, 2190353, 2190354, 2190355, 2190356, 2190357, 2190358, and 2190359 contain(s) the supplementary crystallographic data for this paper. These data are provided free of charge by the joint Cambridge Crystallographic Data Centre and Fachinformationszentrum Karlsruhe Access Structures service.

Chemistry–A European Journal

Research Article
doi.org/10.1002/chem.202202579

Chemistry Europe
European Chemical
Societies Publishing
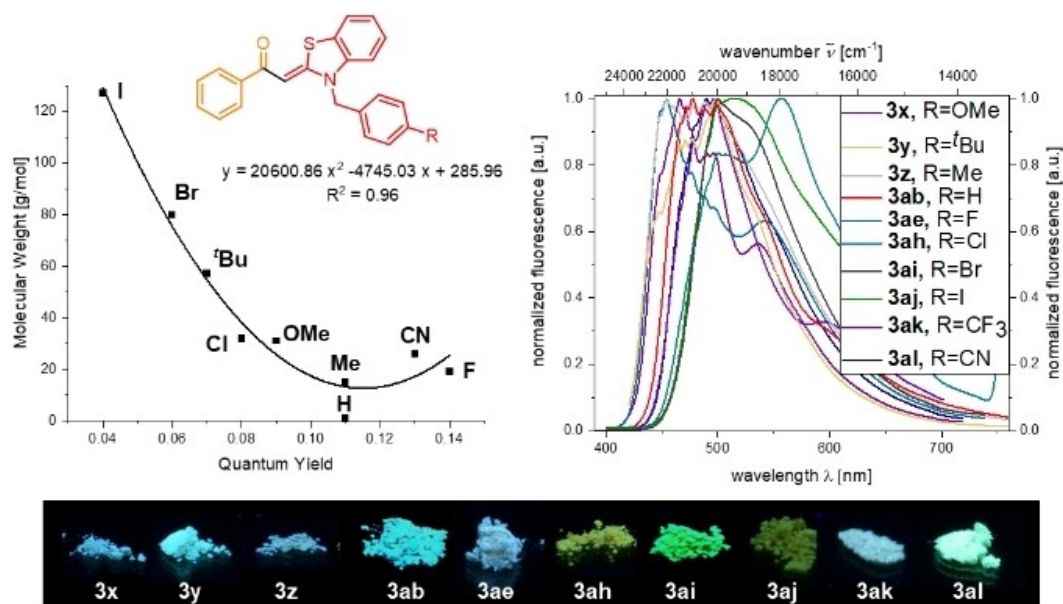
Figure 8. Top left: Correlation between molecular weight and solid-state emission quantum yield of *para*-benzylic-substituted aroyl-*S,N*-ketene acetals **3**. Top right: Normalized solid-state emission spectra of selected aroyl-*S,N*-ketene acetals **3** obtained with a calibrated fluorometer (recorded at $T = 298$ K, $\lambda_{ex} = \lambda_{abs,max}$). Bottom: solid-state fluorescence colors of selected derivatives ($\lambda_{ex} = 365$ nm).
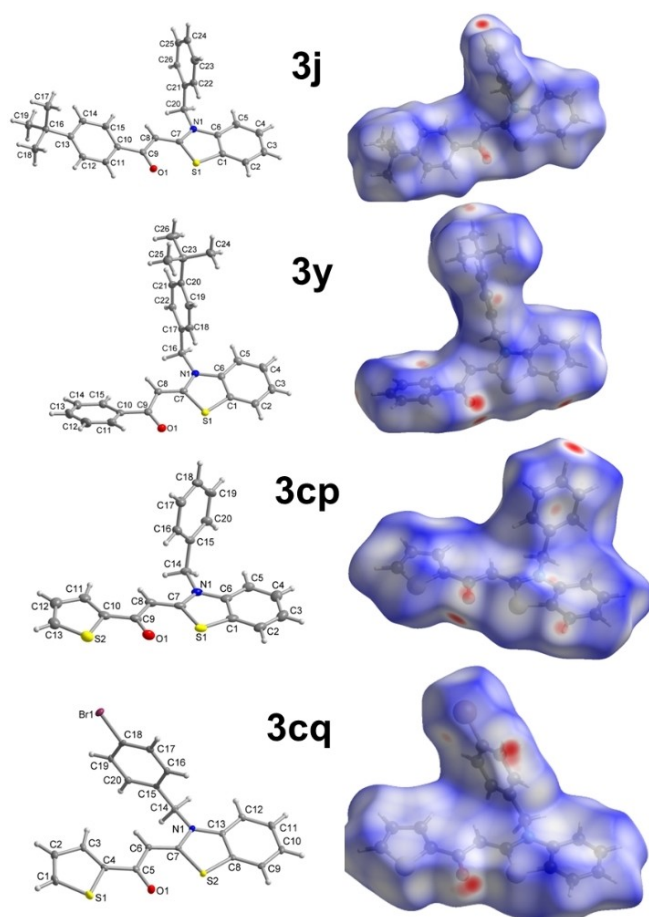
Figure 9. Molecular structures in the solid state (left) and Hirshfeld surfaces (right) of selected acetals.

Influence of substituents at *N*-benzyl moiety

For the solid-state emission quantum yield we observed a remarkable correlation with the substituent at the *para* position of the *N*-benzyl substituent. At first, it must be noted that this substituent has, although only minor, an influence on the solid-state emission color. In this consanguineous series of aroyl-*S,N*-ketene acetals, the most blue shifted example **3 ae** bears a fluorine substituent ($\lambda_{em} = 454$ nm) and the strongest bathochromic shift is observed for *p*-chloro substituted dye **3 ah** ($\lambda_{em} = 557$ nm). For *ortho* and *meta* substitution, we observed an identical behavior as for the *ortho* and *meta* substitution at the aroyl moiety. *Meta* substitution does not change the solid-state quantum yield but the emission maximum is bathochromically shifted. *Ortho* substitution does not influence the emission color but leads to a significantly reduced solid-state quantum yield (Table S8). Upon evaluation of the solid-state emission data, a correlation between the substituent size and the experimentally determined quantum yield can be established. Plotting the quantum yields against the molecular weight of the substituent as a representative measure of its size, we obtain a quadratic correlation function namely $f(x) = 20600.86\,x^2 - 4745.03\,x + 285.96$. An excellent r^2 confirms this correlation (Figure 8) as well as additional crystallographic investigations.

However, this correlation cannot be employed in the case of secondary chromophores as for *N*-naphthyl or trimethoxy benzyl groups, which tend to further increase the solid-state quantum yield. Therefore, taking into account our qualitative approach on the effects of different substituents, we synthesized derivative **3 aq** bearing *N*-trimethoxy benzyl substituent as well as two methyl substituents at the benzothiazole thus generating the aroyl-*S,N*-ketene acetal with the by far highest solid-state quantum yield with $\Phi_f = 0.78$.

Consequently, whatever photophysical property of an aroyl-*S,N*-ketene acetal is required, just the set of postulated rules need to be applied. As only the substitution influence is exemplarily outlined,

Chem. Eur. J. **2022**, *28*, e202202579 (9 of 12)

© 2022 The Authors. Chemistry - A European Journal published by Wiley-VCH GmbH

Chemistry–A European Journal

Research Article
doi.org/10.1002/chem.202202579

Chemistry Europe
European Chemical
Societies Publishing

the full width of investigated aroyl-*S,N*-ketene acetal library can be seen in Chapters 5 and 6 of the Supporting Information.

For a better understanding of this effect, a closer look was taken at the obtained crystal structure alongside a supramolecular packing analysis by PLATON and Hirshfeld surface in order to get a rationalization of this behavior by analyzing intermolecular interactions like C—H⋯π, C—H⋯O and π-π contacts.[21]

Two consanguineous sets of aroyl-*S,N*-ketene acetals were used, on the one hand **3j** and **3y** with *tert*-butyl substituents placed at the 4-position of the aroyl or the benzyl moiety, and on the other hand thiophenoyl-*S,N*-ketene acetals **3cp** and **3cq** with either unsubstituted or *p*-brominated benzyl moiety (Figure 9).

For dye **3cp** (see Chapter 7 in the Supporting Information), there is an interaction between the carbonyl oxygen and a proton of the benzothiazole core and the *p*-benzyl proton thus underlining the importance of this position. In the case of structure **3cq**, the benzyl moiety is significantly less twisted out of plane of the chromophoric π-system compared to compound **3cp** and no strong but only weak C—H⋯Br interactions were observed for the *p*-bromo substituent. Fingerprint plots for both chromophores showed C—C contacts indicating π-stacking interactions and the supramolecular analysis by PLATON gave a less significant single π-π contact for the structure of **3cp**, and three quite significant ones for the structure of **3cq**. As the only difference between these two structures is the substituent at the *para* position of the benzyl substituent, it can be reasoned that due to a larger substituent at the benzyl moiety, more significant π-π contacts occur, consequently leading to quenching of solid state emission and thus reducing Φ_f (**3cp** ($\Phi_f = 0.11$) versus **3cq** ($\Phi_f = 0.06$)) This holds true to a lesser extent for corresponding dyes **3j** and **3y** as the effect is weakened for *tert*-butyl substituent. Additionally, placing the *tert*-butyl substituent at the *para* position of the aroyl moiety effects the emission as well due to electronic effects as mentioned before thus influencing emission color as well as intensity. However, the occurrence of more significant π-π contacts for larger substituents as exemplified by a bromine substituent correlates with quenching of solid-state emission shows the sublime importance of substitution pattern at the *para* position of the benzyl moiety.

For dye **3j**, the crystal structure revealed a nearly planar chromophore π-system, the benzyl substituent is tilted out of the plane. Supramolecular interaction analysis with PLATON indicated an intermolecular interaction between one of the CH_2 protons and the meta-H atom of the benzyl moiety with the carbonyl oxygen atom and C—H⋯π interactions. The same holds true for structure **3y** but the C—H⋯O and C—H⋯π interactions have wider angles, and the latter are also more numerous (see Chapter 7 in the Supporting Information). In the case of dye **3y**, the aroyl moiety is slightly twisted out of plane in comparison to compound **3j** offering a possible explanation for changed solid state emission behavior of **3y**. C—H⋯π interactions of the chromophore π-system are considerably more pronounced in the case of dye **3y** and are incremental for the solid-state emission.

As a consequence, the correlation between solid state quantum yield and substituent size appears indeed as plausible as demonstrated by crystal structures and supramolecular and Hirshfeld surface analysis and, thus, can be used for the fine tuning of Φ_f.

Finally, the influence of substitution on the different position and the interplay of substituents at the benzyl (R[2]), the benzothiazole (R[3]) and the aroyl moiety (R[1]) has now been discussed and explained thoroughly and are summarized in Figure 10. The substituent influence is rated based on previously discussed effects and categorized in four different specifications: big influence,

medium influence, small influence and a negative influence (decrease). The evaluated factors are the emission intensity and Φ_f, respectively, the emission color and the emission behavior. Furthermore, the trend of substituents on the benzothiazole core on solid state Φ_f, the limits of aroyl-*S,N*-ketene acetal AIE-behavior and consequently which structural motifs enable AIE properties and finally the correlation between the aliphatic chain length and the water fraction at the start of aggregation are presented in order to summarize and illustrate the trends discussed previously.

Conclusion

In summary, a vast library of 111 examples of aroyl-*S,N*-ketene acetals has been synthesized by a standard protocol in mostly good to excellent yields. This library now allows data mining of emission characteristics in the solid and aggregated states, which sets the stage for qualitatively rationalizing the influence of the substitution pattern. Full control of the photophysical properties of this class of chromophores results. Variation of the substituents and their interplay affects emission the color, intensity, and quantum yield both in the aggregate and the solid state. The AIE behavior can now be rigorously controlled and tuned with respect to stability and the occurrence of AIE. Supported by crystallographic data, a correlation between substituent size at the benzyl moiety and solid-state quantum yield can be established as well as tools for optimizing the emission output of the dyes. This abundance of aroyl-*S,N*-ketene acetals allows the generation and modification of any desired color from deep blue to near infra-red in the solid-state and in aggregated form. This fruitful concept based on aroyl-*S,N*-ketene acetals as well as implementing them in multi-component reaction methodology allows considerable expansion of the application profile of this class of merocyanine dyes, which is currently under way.

Conflict of Interest

The authors declare no conflict of interest.

Data Availability Statement

The data that support the findings of this study are available from the corresponding author upon reasonable request.

Chemistry–A European Journal

Research Article
doi.org/10.1002/chem.202202579

Chemistry
Europe
European Chemical
Societies Publishing

Figure 10. Influence of substitution sites of aroyl-*S,N*-ketene acetals on solid-state emission (top left) and AIE (top right) behavior, correlation of solid-state quantum yield and substituents at benzothiazole core (bottom left), AIE window of aroyl-*S,N*-ketene acetals (bottom middle), and correlation between aliphatic chain length at aroyl moiety and the water fraction at the starting point of aggregation (bottom right).

[1] M. Saeed, M. Munir, Z. Khalid, S. Ullah, M. Murtaza, G. Farid, T. Rehman, A. Umar, M. M. Elmaadawy, *Appl. J. Environ. Eng. Sci.* **2019**, *5*, 2099–2112.

[2] Y. Q. Sun, J. Liu, X. Lv, Y. Liu, Y. Zhao, W. Guo, *Angew. Chem. Int. Ed.* **2012**, *51*, 7634–7636; *Angew. Chem.* **2012**, *124*, 7752–7754.

[3] a) Q. Hu, M. Gao, G. Feng, B. Liu, *Angew. Chem. Int. Ed.* **2014**, *53*, 14225–14229; *Angew. Chem.* **2014**, *126*, 14449–14453; b) Y. Yuan, S. Xu, X. Cheng, X. Cai, B. Liu, *Angew. Chem. Int. Ed.* **2016**, *55*, 6457–6461; *Angew. Chem.* **2016**, *128*, 6567–6571; c) Q. Li, Y. Li, T. Min, J. Gong, L. Du, D. L. Phillips, J. Liu, J. W. Lam, H. H. Sung, I. D. Williams, *Angew. Chem. Int. Ed.* **2020**, *132*, 9557–9564.

[4] a) D. Liu, J. Y. Wei, W. W. Tian, W. Jiang, Y. M. Sun, Z. Zhao, B. Z. Tang, *Chem. Sci.* **2020**, *11*, 7194–7203; b) M. Shimizu, Y. Takeda, M. Higashi, T. Hiyama, *Angew. Chem. Int. Ed.* **2009**, *48*, 3653–3656; *Angew. Chem.* **2009**, *121*, 3707–3710; c) A. Wakamiya, K. Mori, S. Yamaguchi, *Angew. Chem. Int. Ed.* **2007**, *46*, 4273–4276; *Angew. Chem.* **2007**, *119*, 4351–4354.

[5] F. Gomollón-Bel, *Chem. Int.* **2019**, *41*, 12–17.

[6] a) J. Mei, N. L. Leung, R. T. Kwok, J. W. Lam, B. Z. Tang, *Chem. Rev.* **2015**, *115*, 11718–11940; b) J. Mei, Y. Hong, J. W. Lam, A. Qin, Y. Tang, B. Z. Tang, *Adv. Mater.* **2014**, *26*, 5429–5479; c) Y. Hong, J. W. Y. Lam, B. Z. Tang, *Chem. Commun.* **2009**, *2009*, 4332–4353; d) F. Würthner, *Angew. Chem. Int. Ed.* **2020**, *59*, 14192–14196; *Angew. Chem.* **2020**, *132*, 14296–14301.

[7] B.-K. An, S.-K. Kwon, S.-D. Jung, S. Y. Park, *J. Am. Chem. Soc.* **2002**, *124*, 14410–14415.

[8] a) Y. Tu, Z. Zhao, J. W. Lam, B. Z. Tang, *Nat. Sci. Rev.* **2021**, *8*, nwaa260; b) N. L. Leung, N. Xie, W. Yuan, Y. Liu, Q. Wu, Q. Peng, Q. Miao, J. W. Lam, B. Z. Tang, *Chem. Eur. J.* **2014**, *20*, 15349–15353.

[9] a) C. Li, W.-L. Gong, Z. Hu, M. P. Aldred, G.-F. Zhang, T. Chen, Z.-L. Huang, M.-Q. Zhu, *RSC Adv.* **2013**, *3*, 8967–8972; b) Q. Peng, Z. Shuai, *Aggregate* **2021**, *2*, e91.

[10] a) T. Feng, Q. Zeng, S. Lu, X. Yan, J. Liu, S. Tao, M. Yang, B. Yang, *ACS Photonics* **2018**, *5*, 502–510; b) Z. Zhang, B. Xu, J. Su, L. Shen, Y. Xie, H. Tian, *Angew. Chem. Int. Ed.* **2011**, *50*, 11654–11657; *Angew. Chem.* **2011**, *123*, 11858–11861.

[11] a) L. Yuan, W. Lin, Y. Yang, H. Chen, *J. Am. Chem. Soc.* **2012**, *134*, 1200–1211; b) J. Vogelsang, T. Cordes, C. Forthmann, C. Steinhauer, P. Tinnefeld, *Proc. Natl. Acad. Sci. USA* **2009**, *106*, 8107–8112; c) S. Yang, P. A. Yin, L. Li, Q. Peng, X. Gu, G. Gao, J. You, B. Z. Tang, *Angew. Chem. Int. Ed.* **2020**, *59*, 10136–10142; *Angew. Chem.* **2020**, *132*, 10222–10228; d) X. Huang, L. Qian, Y. Zhou, M. Liu, Y. Cheng, G. Wu, *J. Mater. Chem. C* **2018**, *6*, 5075–5096.

[12] a) B. Xu, Y. Mu, Z. Mao, Z. Xie, H. Wu, Y. Zhang, C. Jin, Z. Chi, S. Liu, J. Xu, *Chem. Sci.* **2016**, *7*, 2201–2206; b) P. Duan, N. Yanai, Y. Kurashige, N. Kimizuka, *Angew. Chem. Int. Ed.* **2015**, *127*, 7654–7659.

[13] a) S. Suzuki, S. Sasaki, A. S. Sairi, R. Iwai, B. Z. Tang, G. i. Konishi, *Angew. Chem. Int. Ed.* **2020**, *132*, 9940–9951; b) B. Huang, W. C. Chen, Z. Li, J. Zhang, W. Zhao, Y. Feng, B. Z. Tang, C. S. Lee, *Angew. Chem. Int. Ed.* **2018**, *130*, 12653–12657; c) R. Iwai, S. Suzuki, S. Sasaki, A. S. Sairi, K. Igawa, T. Suenobu, K. Morokuma, G. i. Konishi, *Angew. Chem. Int. Ed.* **2020**, *132*, 10653–10660.

[14] a) Z. Zhao, J. W. Lam, B. Z. Tang, *J. Mater. Chem.* **2012**, *22*, 23726–23740; b) Z. Zhao, C. Y. Chan, S. Chen, C. Deng, J. W. Lam, C. K. Jim, Y. Hong, P. Lu, Z. Chang, X. Chen, *J. Mater. Chem.* **2012**, *22*, 4527–4534.

[15] a) M. Denißen, N. Nirmalananthan-Budau, T. Behnke, K. Hoffmann, U. Resch-Genger, T. J. J. Müller, *J. Mater. Chem.* **2017**, *1*, 2013–2026; b) M. Denißen, R. Hannen, D. Itskalov, L. Biesen, N. Nirmalananthan-Budau, K. Hoffmann, G. J. Reiss, U. Resch-Genger, T. J. J. Müller, *Chem. Commun.* **2020**, *56*, 7407–7410; c) A.-L. Elsner, L. Biesen, T. J. J. Müller, *Arkivoc* **2021**, *3*, 53–66; d) F. Wilbert, T. J. J. Müller, *Dyes Pigm.* **2022**, *198*, 109938.

[16] a) N. Nirmalananthan, T. Behnke, K. Hoffmann, D. Kage, C. F. Gers-Panther, W. Frank, T. J. J. Müller, U. Resch-Genger, *J. Phys. Chem. C* **2018**, *122*, 11119–11127; b) F. K. Merkt, T. J. J. Müller, *Sci. China Chem.* **2018**, *61*, 909–924; c) L. Biesen, T. J. J. Müller, *Adv. Synth. Catal.* **2021**, *363*, 980–1006.

Chemistry–A European Journal

Research Article
doi.org/10.1002/chem.202202579

Chemistry
Europe
European Chemical
Societies Publishing

[17] a) X. Zhang, D. Wang, H. Shen, S. Wang, Y. Zhou, Y. Lei, W. Gao, M. Liu, X. Huang, H. Wu, *Org. Chem. Front.* **2021**, *8*, 856–867; b) Y. Chen, Y. Xie, H. Shen, Y. Lei, Y. Zhou, W. Dai, Z. Cai, M. Liu, X. Huang, H. Wu, *Chem. Eur. J.* **2020**, *26*, 17376–17380; c) X. Zhang, D. Wang, Y. Lei, M. Liu, Z. Cai, H. Wu, G. Shen, X. Huang, Y. Dong, *Chem. Commun.* **2022**, *58*, 1179–1182; d) Y. Guo, K. Chen, Z. Hu, Y. Lei, X. Liu, M. Liu, Z. Cai, J. Xiao, H. Wu, X. Huang, *J. Phys. Chem. Lett.* **2022**, *13*, 7607–7617; e) X. Han, K. Chen, Y. Lei, J. Huang, S. Wie, Z. Cai, H.-Y. Wu, M.-C. Liu, X.-B. Huang, Y. Dong, *ACS Materials Lett.* **2022**, *4*, 1764–1773.

[18] L. Biesen, N. Nirmalananthan-Budau, K. Hoffmann, U. Resch-Genger, T. J. J. Müller, *Angew. Chem. Int. Ed.* **2020**, *59*, 10037–10041; *Angew. Chem.* **2020**, *132*, 10123–10127.

[19] a) L. Biesen, L. May, N. Nirmalananthan-Budau, K. Hoffmann, U. Resch-Genger, T. J. J. Müller, *Chem. Eur. J.* **2021**, *27*, 13426–13434; b) L. Biesen, T. J. J. Müller, *Aggregate* **2021**, *2*, e105.

[20] L. Biesen, J. Krenzer, N. Nirmalananthan-Budau, U. Resch-Genger, T. J. J. Müller, *Chem. Sci.* **2022**, *13*, 5374–5381.

[21] a) A. L. Spek, *Acta Crystallogr. Sect. D* **2009**, *65*, 148–155; b) M. A. Spackman, D. Jayatilaka, *CrystEngComm* **2009**, *11*, 19–32; c) J. J. McKinnon, D. Jayatilaka, M. A. Spackman, *Chem. Commun.* **2007**, 3814–3816; d) F. L. Hirshfeld, *Theor. Chim. Acta* **1977**, *44*, 129–138.